PHILOSOPHICAL TRANSACTIONS A

rsta.royalsocietypublishing.org

Research

Cite this article: England P, Howell A, Jackson J, Synolakis C. 2015 Palaeotsunamis and tsunami hazards in the Eastern Mediterranean. *Phil. Trans. R. Soc. A* **373**: 20140374.
http://dx.doi.org/10.1098/rsta.2014.0374

Accepted: 8 June 2015

One contribution of 14 to a theme issue 'Tsunamis: bridging science, engineering and society'.

Subject Areas:
geophysics

Keywords:
tsunami, earthquake, East Mediterranean

Author for correspondence:
Philip England
e-mail: philip.england@earth.ox.ac.uk

Electronic supplementary material is available at http://dx.doi.org/10.1098/rsta.2014.0374 or via http://rsta.royalsocietypublishing.org.

Palaeotsunamis and tsunami hazards in the Eastern Mediterranean

Philip England[1], Andrew Howell[2], James Jackson[2] and Costas Synolakis[3,4]

[1]Department of Earth Sciences, University of Oxford, South Parks Road, Oxford OX1 3AN, UK
[2]Department of Earth Sciences, Bullard Laboratories, Madingley Road, Cambridge CB3 0EZ, UK
[3]School of Environmental Engineering, Technical University of Crete, 73100 Chania, Crete, Greece
[4]Viterbi School of Engineering, University of Southern California, Los Angeles, CA 90089-2531, USA

CS, 0000-0003-0140-5379

The dominant uncertainties in assessing tsunami hazard in the Eastern Mediterranean are attached to the location of the sources. Reliable historical reports exist for five tsunamis associated with earthquakes at the Hellenic plate boundary, including two that caused widespread devastation. Because most of the relative motion across this boundary is aseismic, however, the modern record of seismicity provides little or no information about the faults that are likely to generate such earthquakes. Independent geological and geophysical observations of two large historical to prehistorical earthquakes, in Crete and Rhodes, lead to a coherent framework in which large to great earthquakes occurred not on the subduction boundary, but on reverse faults within the overlying crust. We apply this framework to the less complete evidence from the remainder of the Hellenic plate boundary zone, identifying candidate sources for future tsunamigenic earthquakes. Each such source poses a significant hazard to the North African coast of the Eastern Mediterranean. Because modern rates of seismicity are irrelevant to slip on the tsunamigenic faults, and because historical and geological data are too sparse, there is no reliable basis for a probabilistic assessment of this hazard, and a precautionary approach seems advisable.

THE ROYAL SOCIETY PUBLISHING

1. Introduction

The assessment of tsunami hazard in the Eastern Mediterranean has been severely hampered by uncertainty in the locations and magnitudes of the causative earthquakes; in consequence a wide range of calculated scenarios exists for tsunamigenic earthquakes in the region (e.g. [1–5]). The two most devastating historical tsunamis recorded in the region, those of AD 365 and AD 1303, were probably generated by large or great (magnitude $\gtrsim 7$ or magnitude > 8) earthquakes at the Hellenic plate boundary (e.g. [6,7]). There is strong geological evidence that the AD 365 tsunami was caused by an earthquake in western Crete (e.g. [8–12]) and that another tsunamigenic earthquake occurred near Rhodes in prehistorical or Roman times [13–16]. Attempts to identify other source locations along the Hellenic plate boundary have relied on analogies with major subduction zones around the world, and have defined source parameters on the basis of the seismicity of the past few decades. The complexity of this plate boundary zone, and the fact that most of the convergence across it is aseismic [17], suggest that the seismicity data, alone, are a misleading guide to likely sources of tsunamigenic earthquakes. Instead, we develop a model that takes advantage of recent understanding of the tsunami hazard at this plate boundary, which has developed by combining geological, geophysical, geodetic, geomorphological, geochronological and historical data (e.g. [10,12,13,18–21]).

2. Tectonic setting

The Hellenic plate boundary zone accommodates approximately 40 mm yr^{-1} of relative motion between the oceanic lithosphere of the Eastern Mediterranean (part of the Nubian plate) and the continental lithosphere of Greece and the Aegean Sea [21–23]. Approximately three-quarters of this motion arises from distributed deformation within the continental lithosphere of Greece and Turkey, which causes the southern Aegean to move southwestwards with respect to stable Eurasia at approximately 30 mm yr^{-1} [24,25]. The lithosphere of the Aegean region undergoes horizontal extension, as is shown by pervasive normal faulting (figure 1*a*, [31]). In the southernmost Aegean, earthquakes, active faulting and GPS data show along-arc extension (figure 1, [19,20,32–34]), which, combined with the change in strike of the plate boundary zone from NW–SE in the west to almost SW–NE in the east, causes the relative motion across the boundary to vary from almost pure convergence in the west to highly oblique convergence in the east (figure 1*b*).

Studies of the release of seismic moment in the region over the instrumental period [17] and of the relative motions recorded by GPS measurements [21] suggest that less than 20% of the relative motion takes place in earthquakes, with the remainder taking place by aseismic slip. To accommodate the relative motion seismically would require an M8 earthquake approximately once per century and, although the historical record is incomplete, it is inconceivable that the approximately 20 great earthquakes that would be needed to remove the deficit during the past 2000 years could have occurred unremarked [6,17]. But the historical record does indicate that two or three great earthquakes occurred at this boundary during this interval of time [6]. Because there is no known place where a fault that slips predominantly aseismically also fails in occasional great earthquakes, the logical conclusion to draw is that great earthquakes in the Hellenic plate boundary zone occur not on the subduction fault but on another fault or faults within the zone [10].

The complex morphology of the region makes the identification of those faults difficult. Most subduction zones exhibit a steep-sided bathymetric low, the trench, which marks the projection to the surface of the subduction fault. The subduction fault in the Hellenic plate boundary zone does not crop out; its closest approach to the surface probably lies beneath the broad bathymetric high of the Mediterranean Ridge (figure 1), a prism of sediments about 10 km thick [35–37]. Deep (approx. 4000 m.b.s.l.) linear features are, however, visible in the bathymetry of the Hellenic plate boundary, in particular the Hellenic, Pliny and Strabo Trenches (figure 1*a*). These features are not, despite their names, trenches in the plate-tectonic sense but probably represent the outcrop of

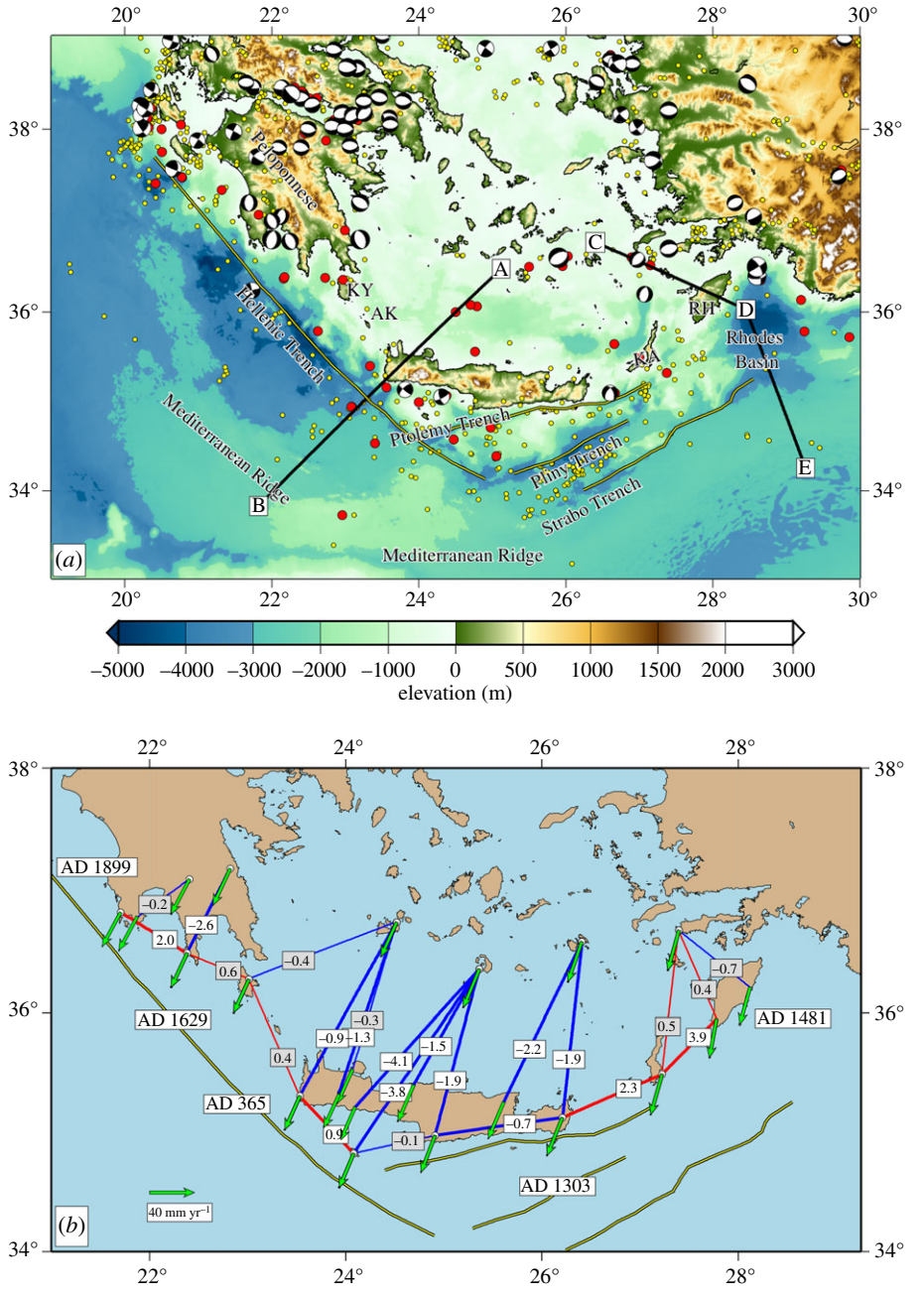

Figure 1. The Hellenic plate boundary zone. (*a*) Topography (colour scale at the bottom) and locations discussed in the text. AK, Antikythera; KY, Kythera; KA, Karpathos; RH, Rhodes. Dots show the epicentres of shallow (depth < 30 km) earthquakes for 1960–2010 from the EHB catalogue [26,27] and for 1900–1999 from the catalogue of Engdahl & Villaseñor [28]; yellow and red dots show earthquakes with magnitudes, respectively, less than 5.8 and greater than or equal to 5.8. Focal mechanisms are of earthquakes within the upper crust of the Eurasian lithosphere [20,29,30]. The lines AB and CDE show the locations of sections in figure 3. (*b*) Relative motions between the Aegean and Nubia. Green arrows show the velocities of GPS sites in the Peloponnese and the islands of the southern Aegean with respect to the Nubian plate; the velocities of [22] are rotated into the Nubian frame using the pole of [23]. Baselines between GPS sites are shown by red (lengthening) and blue (contracting) lines. Rates of change of length of line (mm yr^{-1}) are shown in boxes. Thicker lines and white boxes correspond to baselines whose length changes are greater than their 1σ uncertainties; thinner lines and grey boxes denote length changes that are not resolved at the 1σ level. Dates (AD 365–AD 1899) refer to approximate source regions of tsunamigenic earthquakes discussed in §3.

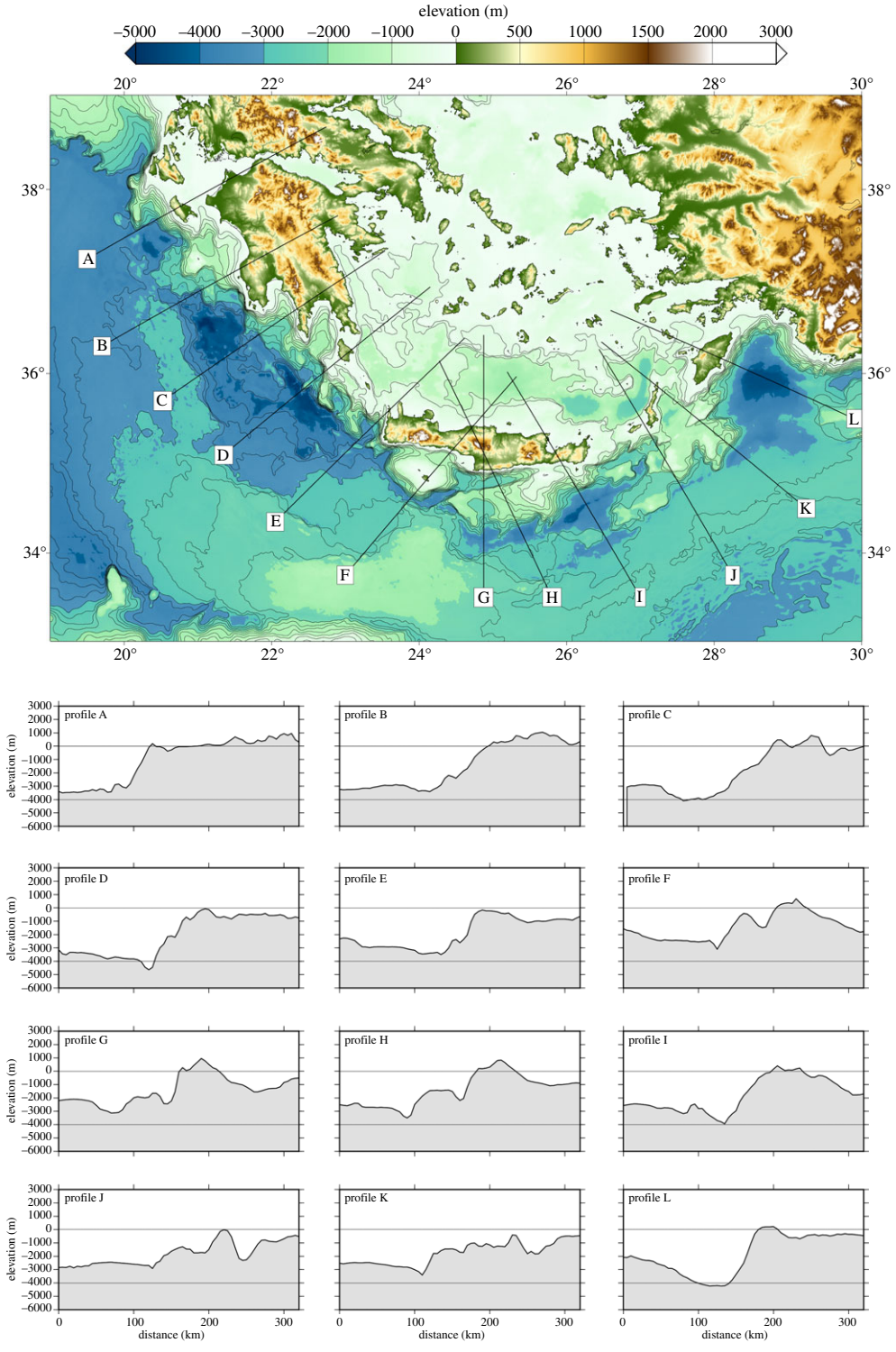

Figure 2. Profiles of bathymetry along 12 sections perpendicular to the Hellenic, Pliny and Strabo Trenches.

major faults within the deforming sedimentary wedge on top of the Nubian plate [10,20,36,38–41]. While the Hellenic Trench is generally considered to represent the outcrop of a reverse fault, the Pliny and Strabo Trenches (figure 1*a*) have been interpreted as the expressions of normal

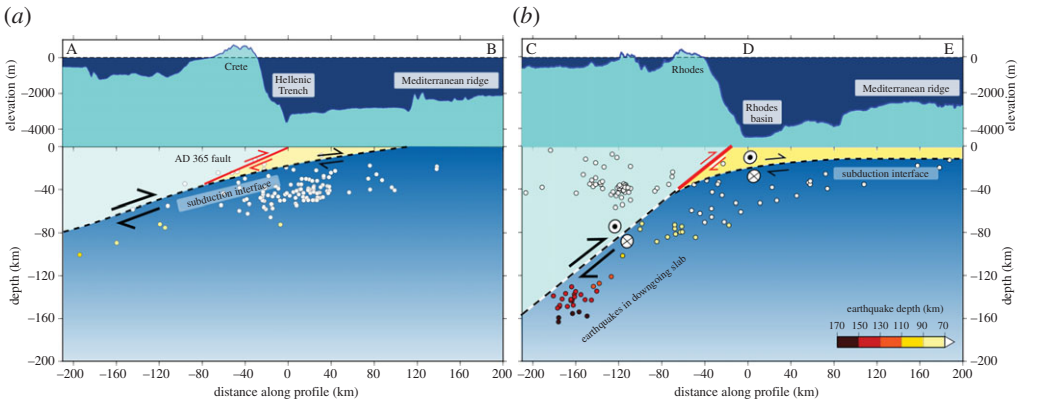

Figure 3. Sketches of the configuration of faulting in the Hellenic plate boundary, after [10,13]. The locations of the sections are shown in figure 1*a*. The lithosphere of the south Aegean and its underlying upper mantle are shown to the left of each panel in light blue; Nubian lithosphere and its upper mantle are shown to the right in darker blue. At the top of each panel, topography is shown at an exaggerated scale. Yellow shading represents the thick sedimentary pile on top of the Mediterranean sea floor. The subduction interface is shown by the dashed line separating the Nubian plate from the overlying sediment and the Aegean lithosphere. In each profile, the rate of slip on the subduction boundary decreases towards the surface, leading to contractional strain (seen in the GPS data of figure 1*b*) that is released in reverse faulting at the locations shown in red.

faulting [42], strike-slip faulting [43,44], reverse faulting [20,45] and various combinations of these (e.g. [36,40,46,47]).

The bathymetric profiles across the Hellenic, Pliny and Strabo Trenches, and across the north edge of the Rhodes Basin, show strong similarities that suggest that these features may have a common origin (figure 2). In each case, the depth of the ocean floor increases northwards of the Mediterranean Ridge towards the trenches, with maximum depths of 3000–4500 m occurring close to the continental margin of the Peloponnese and the Aegean Sea. The profiles are also strongly asymmetric, with steep slopes on the landward sides, a form that is characteristic of topographic profiles perpendicular to major reverse faults. The similarities between the profiles are paradoxical because the direction of overall relative motion across this region varies from pure convergence in the west to highly oblique in the east (figure 1*b*). Howell *et al.* [13] suggest that the paradox may be resolved if relative motion across the eastern part of the plate boundary is partitioned into arc-parallel slip along the subduction interface and arc-perpendicular reverse faulting that crops out on the trenches within the over-riding Aegean crust (figure 3).

This suggestion is supported by the slip vectors of the few earthquakes along the subduction fault for which focal mechanisms may be determined [13,20,48], and by the relative velocities of GPS sites in the southernmost Aegean ([21–23,25], figure 1*b*). While baselines parallel to the trench system are generally extending, consistent with the observations of active faulting and focal mechanisms of earthquakes (figure 1, [19,32]), baselines perpendicular to the trenches are generally shortening. Thus, a small fraction of the convergence rate between the Aegean and Nubia is being accommodated by contractional strain within the Aegean lithosphere [10,21]. In §3, we discuss the evidence suggesting that this contraction is eventually released in occasional large or great earthquakes on reverse faults whose outcrops are marked by the Hellenic, Pliny and Strabo Trenches (figures 1 and 3). In §4, we carry out hydrological simulations of candidate tsunamis generated by such sources.

3. Potential tsunami sources at the Hellenic plate boundary

(a) Historical record

The assessment of tsunami hazard in the Eastern Mediterranean is hampered by the proliferation of tsunami catalogues, many of which are based on secondary or more distant sources, and

which have promulgated a range of errors, including non-existent earthquakes and tsunamis. Comparing these catalogues with the historical record, Ambraseys & Synolakis [7] rejected 65 out of 75 alleged historic tsunamis between AD 66 and 1928. Half of the historical reports rejected by Ambraseys & Synolakis [7] either were not based on historical sources, or the sources had been interpreted 'with a tinge of imagination'. The remaining incorrect attributions of tsunamis represent inundations that were probably caused by local effects, including storm surges (see also [49]). We refer the reader to detailed analysis of the historical record [6,7,49] for a wider discussion of the pitfalls in its interpretation.

Five reliable historical reports of tsunamis are closely associated with earthquakes along the Hellenic plate boundary: 21 July AD 365, Crete; 8 August AD 1303, Crete; 3 May AD 1481, Rhodes; 28 February AD 1629, Kythera; and 22 January, AD 1899, Kyparissia. The approximate locations of these events are shown in figure 1*b*.

(b) The AD 365 earthquake and tsunami

The historical evidence for the devastation of Alexandria and surrounding regions by a tsunami on 21 July AD 365 is well established [6,50,51]. The tsunami has long been attributed, on the basis of uplifted indicators of past sea level or 'sea marks', to an earthquake whose epicentre lay near western Crete (e.g. [9,11,12,52,53]). Recent analysis shows that these observations can be combined with geochronological, geomorphological, seismological and geodetic data into a coherent model of the AD 365 earthquake that is consistent with the historical record [10]. Evidence of tsunamigenic potential for the other parts of the Hellenic plate boundary is patchy, so in this paper we use western Crete as the 'Rosetta Stone' through which the incomplete evidence from other parts of the Hellenic plate boundary may be interpreted.

m The 'sea marks' around the shore of western Crete were first described by Capt. Thomas Spratt [54] who, during a hydrological survey of Crete, identified features formed at or below sea level that had been raised up to 10 m.a.s.l. in historical time. These features include bio-erosional notches, algal encrustations and other remains of marine species that are found in life position [9,53]. Their highest level is often marked by a prominent algal encrustation that is not seen elsewhere on the cliffs below, except where similar constructions are found growing at present sea level [10]. In what follows we shall, for brevity, refer to the uppermost levels of these marine features as palaeoshorelines. To our knowledge, in all places where such a palaeoshoreline is found, this level also marks a clear transition between (above) rock that has experienced long-lived sub-aerial erosion and (below) submarine erosion or marine encrustation. The palaeoshorelines are therefore interpreted as having been formed during the interval between the stabilization of sea level, approximately 6000 years before present (6 ky BP), and the events that lifted them.

Before the recent advances in radiocarbon dating, which allowed the determination of high-precision ages from small samples, the timing of the uplift events was uncertain; indeed the radiometric dates allowed the possibility that the palaeoshorelines were uplifted in a series of small events (e.g. [9,15,53,55]). Recent high-precision radiocarbon dates from corals preserved between present sea level and the palaeoshorelines in western Crete show, however, that at least 75%, and probably more than 90%, of the post-6 ky BP uplift took place in a single event, which was contemporaneous, within the uncertainty of radiocarbon dating, with the AD 365 earthquake [10].

The elevations of the palaeoshorelines in western Crete die off smoothly with distance measured northeastwards from the southwest corner of Crete, and this distribution of uplift (observations of Pirazzoli *et al.* [9] and Shaw *et al.* [10], figure 4) is consistent with slip of about 20 m on a fault that dips at about 30° and crops out at the Hellenic Trench [10]. The along-strike length of the fault break is constrained by the absence of uplifted shorelines on Kythera and Gavdos (figure 4) to be about 100 km [10]. Shaw *et al.* [10] assumed that the fault slipped from the surface to a depth of 45 km, and from their fault parameters they arrived at an estimated magnitude of $M_w = 8.3–8.5$. Independently, Papadimitriou & Karakostas [8] inferred the parameters of the

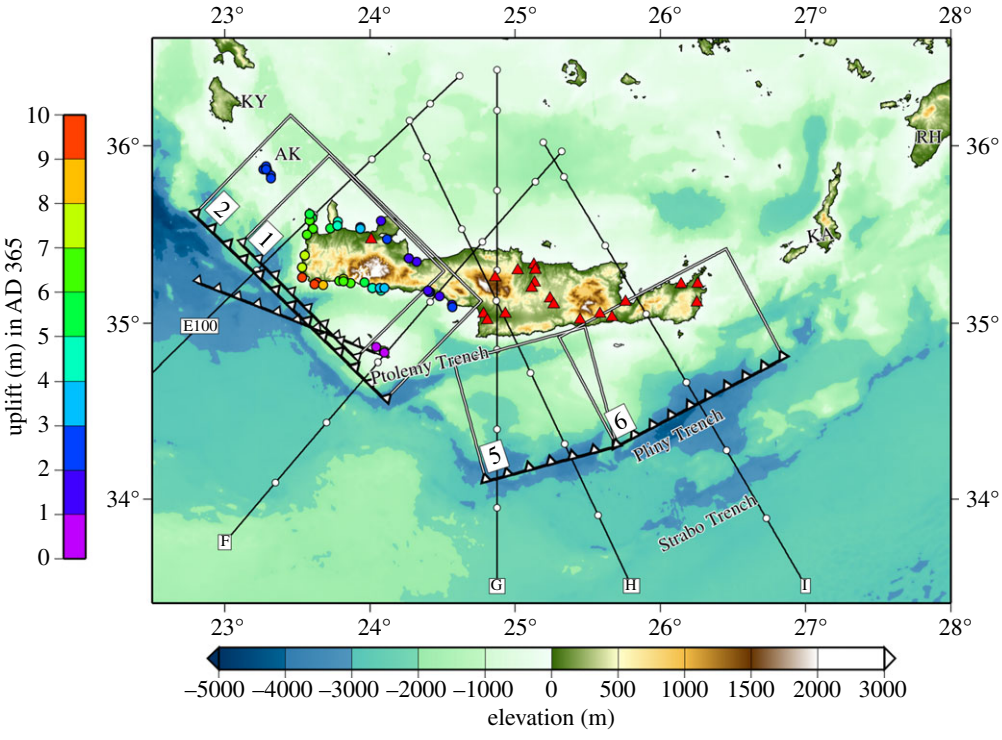

Figure 4. Location map for potential tsunami sources near Crete. Coloured circles (scale to left) show the observed elevations above present sea level of palaeoshorelines lifted by the earthquake of AD 365 [9,10]. Rectangles with fault symbols show the projection on the surface of fault sources used in this study: 1, location of AD 365 earthquake inferred by Shaw *et al.* [10]; 2, location of AD 365 earthquake inferred by Papadimitriou & Karakostas [8]. Tsunami simulations for these sources are illustrated in figure 6. Planes 5 and 6 show locations of model sources for the tsunami simulations illustrated in figure 8. Fault symbol without accompanying rectangle shows the location of the AD 365 event inferred by Stiros & Drakos [12]; this plane dips NNE at 40° to a depth of 70 km. Red triangles show the locations of substantial Minoan edifices that suffered earthquake damage in Late Minoan IA time [56]. The lines of profiles E–I (figure 2) are decorated with white dots at intervals of 50 km from their southern ends; the label E100 is at 100 km from the southern end of profile E.

AD 365 earthquake using the smaller dataset of Pirazzoli *et al.* [9]. They found a fault of length 160 km dipping at 30° to a depth of 50 km and, imposing a moment of $M_w = 8.3$, solved for a distribution of slip on the fault plane (figure 4). The observations of uplift can also be fitted by slip on a fault that strikes at an angle of approximately 30° to the Hellenic Trench and dips at about 40° to a depth of 70 km [12].

Although the range of fault parameters is consistent with the observations of uplift and with the strike of the major bathymetric features of the region, the uplift is inconsistent with slip on the plate interface (see fig. 1 of supplementary material of [10]). In our tsunami simulations (figure 6), we use the sources of Shaw *et al.* [10] and Papadimitriou & Karakostas [8] to investigate the impacts of uncertainties in source size. We do not illustrate the source suggested by Stiros & Drakos [12], which cuts across the principal bathymetric features of the region and seems unlikely to correspond to an active fault.

(c) Evidence from other parts of the plate boundary zone

(i) Rhodes

The eastern coast of Rhodes exhibits a set of palaeoshorelines that share many characteristics with those uplifted in western Crete in AD 365 [14,15]. Their maximum elevations are, however, lower

than 4 m and their distribution has been disturbed by relative vertical motions across normal faults that are both perpendicular to [15] and parallel to [13] the uplifted shorelines. The event that lifted up the shorelines is estimated, from the ^{14}C ages of lithophagid shells found between the palaeoshorelines and modern sea level, to have occurred in the interval 1600–1100 BC [13]. The youngest ^{14}C age from the lithophagids yields a 2σ range of 3950–3450 BP (2000–1500 BC) but this range may place the date of the earthquake up to 400 years too early, because lithophagids appear to incorporate small amounts of older carbon from their substrate into their shells [57]. The uplift of the shorelines has also been attributed, on the basis of an uplifted slipway, to the famous earthquake of *ca* 227 BC that destroyed the Colossus of Rhodes [16].

The morphological similarities between the approximate 6 ky BP palaeoshorelines in Rhodes and western Crete strongly suggest that, as in Crete, the uplift in Rhodes took place in a single event. For our present purpose, it is unimportant whether that uplift was in the third century BC [16] or in late Bronze Age time [13]. Some of the lithophagids whose ^{14}C dates place uplift in the Bronze Age were collected within about 1 m of present sea level; it therefore seems likely that, whatever the age of the main uplift, the AD 1303 and AD 1481 earthquakes caused negligible subsequent uplift of the shorelines.

(ii) Eastern Crete

Although there is widespread evidence of uplift of the shores of eastern Crete, we are not aware of any palaeoshoreline, such as those in Rhodes and western Crete, that would suggest uplift by a single seismic event. We should not, however, expect significant coastal uplift associated with large or great earthquakes in this part of the plate boundary, because the coast lies close to the maximum down-dip extent of slip on likely fault sources (figure 4). The observed uplift may result from the uplift of footwalls of the arc-parallel and arc-perpendicular normal faults of the region, though there may also be a regional component to the uplift arising from reverse faulting (e.g. [19,58,59]).

The tsunami that affected Alexandria in 1303 was probably generated by an earthquake near eastern Crete [6,60]. The ground shaking associated with the AD 1303 earthquake seems to have been concentrated in eastern Crete, though the incompleteness of the historical record means that significant shaking in Rhodes cannot be ruled out [6]. In addition, archaeological evidence of widespread earthquake destruction in important Bronze Age sites [56] suggests that a large or great earthquake occurred near eastern Crete during the period referred to as Late Minoan IA (LMIA). It has been suggested (e.g. [61]) that each site was destroyed by a moderate (magnitude ~ 6) earthquake on a nearby fault. Although the absolute age of LMIA is a perennial matter of dispute between those who accept dates based on radiocarbon and those who do not, the duration of LMIA is agreed to have been about 100 years [62]. Thus, the suggestion of multiple moderate earthquakes [61] requires at least 20 magnitude ~ 6 earthquakes on the island within about 100 years. This seems implausible: for comparison, figure 1*a* shows that no earthquake of magnitude 5.8 or greater was reported beneath eastern Crete between 1900 and 2010.

For our tsunami simulations, we place sources along the Pliny Trench, whose expression, near eastern Crete, is much more pronounced than that of the Strabo Trench (figures 2 and 4). It seems likely that the other bathymetric low in the region, the Ptolemy Trench, represents an extensional graben within the accretionary prism [19,42]. Gallen *et al.* [42] suggest that extensional faulting in the Ptolemy Trench rules out contractional faulting, and its associated earthquake and tsunami hazards, along the south coast of Crete. They draw this inference on the basis that a north-dipping reverse fault cannot crop out adjacent to the south-dipping normal faults near the southern coast of Crete (fig. 7 of [42]); this argument is irrelevant to the reverse faulting that we discuss here, which crops out far offshore. The bathymetric map (figure 4), and topographic profiles G and H (figure 2), suggest that the Pliny and Ptolemy Trenches are an example of the well-understood phenomenon of parallel reverse and normal faulting, with the normal faulting being within crust of greater surface elevation and higher gravitational potential energy (e.g. [63]; see also [64]).

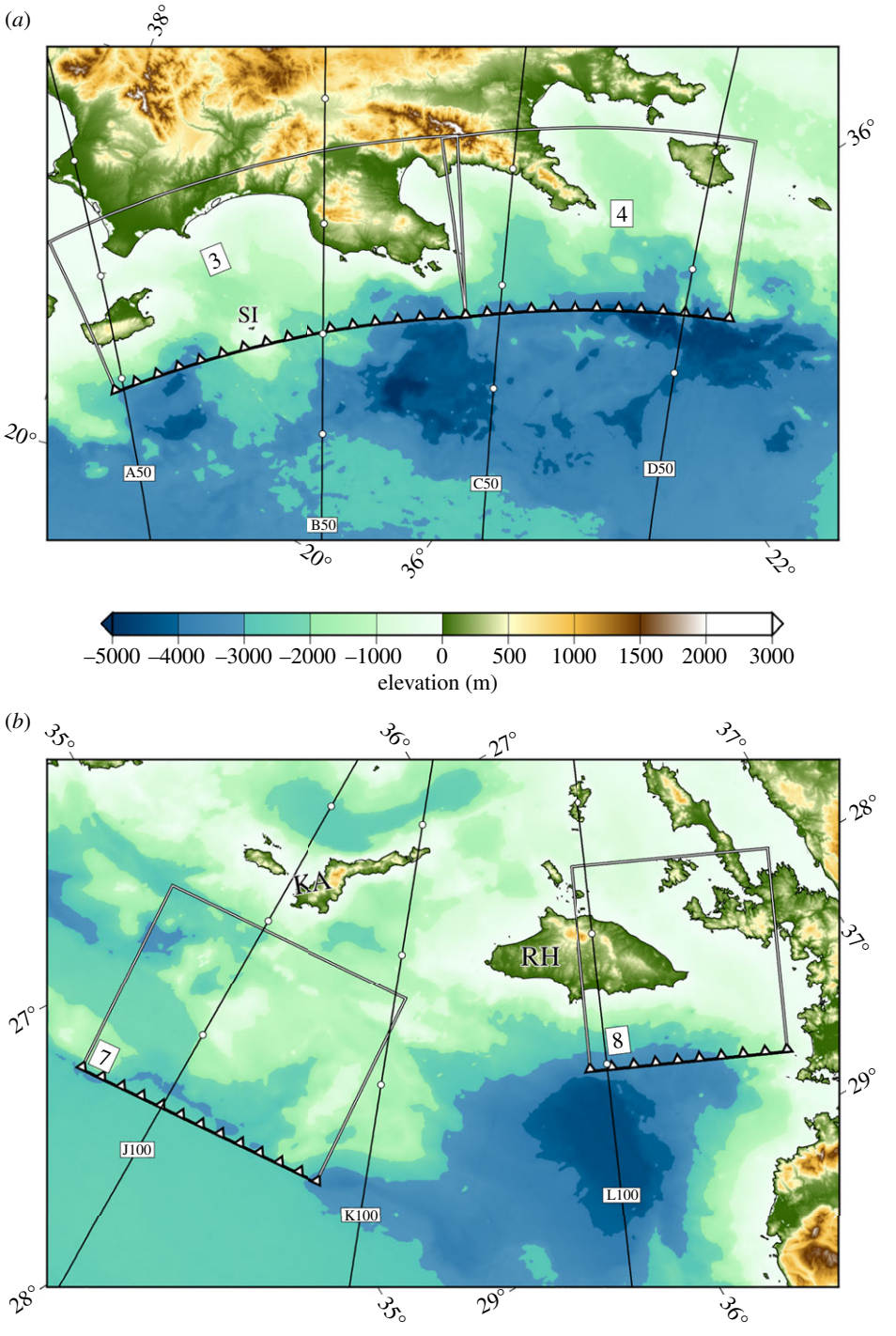

Figure 5. Location map for potential tsunami sources (*a*) near the Peloponnese and (*b*) near the eastern end of the Hellenic plate boundary. Symbols as for figure 4. (*a*) Rectangles and fault symbols show the locations of the model sources near the Peloponnese; the tsunami simulations are illustrated in figure 7. The lines of profiles A–D (figure 2) are decorated with white dots at intervals of 50 km from their southern ends; the label of each profile is given at 50 km from its southern end. (*b*) Rectangles show the locations of the model sources near Karpathos and Rhodes (following [13]); the tsunami simulations are illustrated in figure 9. Numbers refer to sources listed in table 1. The lines of profiles K–L (figure 2) are decorated with white dots at intervals of 50 km from their southern ends; the profiles are labelled at 100 km from their southern ends.

Table 1. The parameters of sources used in the tsunami simulations. The longitudes and latitudes of the intersection of the fault with the surface are given. In each case, slip on the fault is assumed to be in the pure reverse sense (rake = 90°) and the fault has uniform slip from the surface to the depth shown.

	endpoints							
source	°E	°N	°E	°N	dip	slip (m)	depth (km)	figures
1. Western Crete [10]	23.90	34.80	23.11	35.45	30°	20	45	6*a*
2. Western Crete [8]	24.10	34.57	22.79	35.61	35°	20	45	6*b*
3. Peloponnese (north)	21.65	36.50	20.40	37.70	30°	20	45	7*a*
4. Peloponnese (south)	22.60	35.70	21.65	36.50	30°	20	45	7*b*
5. Eastern Crete (west)	25.70	34.30	24.80	34.10	30°	20	45	8*a*
6. Eastern Crete (east)	26.85	34.80	25.70	34.30	30°	20	45	8*b*
7. Karpathos	28.20	35.00	27.30	34.50	30°	20	45	9*a*
8. Rhodes [13]	28.73	36.61	28.38	36.00	35°	9	40	9*b*

We consider the Pliny Trench to be the most probable source of a tsunamigenic earthquake in this region but we do not rule out the possibility of large earthquakes on the Strabo and Ptolemy Trenches, showing calculations for these sources in the electronic supplementary material.

(iii) Peloponnese and Karpathos segments

Evidence for tsunamigenic potential of other parts of the plate boundary is, at present, scarce. The historical record shows two tsunamis associated with earthquakes near the Peloponnese (28 February AD 1629, Kythera, and 22 January, AD 1899, Kyparissia [6,7]), and uplifted notches on the Strophades Islets (SI in figure 5*a*) suggest a large earthquake there about 1500 years ago [65]. The morphological evidence for late-Quaternary uplift of the coast of the Peloponnese [66] suggests that thrusting in this region may be lifting the surface in a fashion analogous to that of western Crete [10]. In the section of the boundary between eastern Crete and Rhodes, which we refer to as the Karpathos segment, the Pliny and Strabo Trenches lie far enough offshore for it to be unlikely that uplift caused even by large earthquakes would be preserved.

Clearly, these observations alone would not justify an insistence that these sections of the plate boundary generate large or great earthquakes. We suggest, however, that, in view of their morphological similarities with other parts of the plate boundary that do generate such earthquakes, it would be unwise to assume that the Peloponnese and Karpathos segments do not generate tsunamigenic earthquakes. Accordingly, we carry out tsunami simulations for the model sources shown in figure 5. Tsunami simulations for alternative choices of source in these regions are shown in the electronic supplementary material.

4. Tsunami simulations

We carried out calculations for the tsunamis generated by slip on the fault segments that are illustrated in figures 4 and 5, and listed in table 1; calculations for alternative sources are shown in the electronic supplementary material. The initial condition for each tsunami simulation is given by a static displacement of the sea floor that is calculated assuming uniform slip of a dislocation in an elastic half-space, using the method of Okada [67] with the relevant source parameters (table 1). The propagation of the tsunami is calculated using the method of splitting tsunami algorithm (MOST, e.g. [68–70]). This method solves the depth-integrated nonlinear shallow-water equation by a finite-difference algorithm that splits the equation, in two spatial dimensions plus time, into a pair of equations in one dimension plus time [70]. MOST has been extensively validated through

the hydrodynamic community's standards [69]. Calculation of the details of inundation or run-up are heavily dependent upon detailed bathymetric models for the near-shore environment, which, except in a few locations, are not available to us. For this reason, the hydrodynamical simulations stop at the 30 m isobath.

The lengths of the fault segments that we use are mostly around 100 km (table 1), in contrast to the lengths of 200 km or more that have been considered in earlier tsunami scenarios for the Eastern Mediterranean (e.g. [1,2,4,5]). The Hellenic Trench is approximately linear for about 400 km, while the Pliny Trench extends for over 200 km. It might, therefore, seem reasonable to postulate that the largest feasible tsunamigenic earthquakes would break the entire lengths of these faults. Indeed, we cannot rule out this possibility, but we concentrate here on potential earthquake sources that are no longer than the 100–150 km derived from analysis of the uplifted shorelines of western Crete and Rhodes [8,10,13,53]. Fault segments of such a length are supported by two further observations. First, changes of 5–10° in the strike of the trenches occur at this scale (figures 4 and 5). Secondly, the crust of the Aegean, which overlies the reverse faults that crop out at the trenches, is broken up by pervasive arc-parallel extensional faulting [19,32]. It seems likely that these faults represent weakness against which rupture may terminate, as observed by Oldham [71] in the great 1897 Assam earthquake, which had similar rupture parameters to the AD 365 earthquake [10,72]. Indeed, Papadimitriou & Karakostas [8] assume that such segmentation governed the extent of the AD 365 rupture.

For source 8, near Rhodes, we adopt the parameters given by Howell *et al*. [13] (table 1); for the remaining sources, we assume that slip takes place from the surface to a depth of 45 km. This assumption is supported by the analysis of Shaw *et al*. [10] for the AD 365 earthquake, and by the observation that hypocentres of micro-earthquakes within the over-riding plate are shallower than around 45 km [73,74]. This depth is also the maximum extent of shallowly dipping thrust faulting on the subduction interface [20], as is common in subduction zones [75]. We adopt a uniform slip of 20 m, as estimated for the AD 365 earthquake. Although the lengths of the fault segments are of the order of 100 km, and therefore the ratio of slip to length that we assume is higher than generally observed in earthquakes (e.g. [76]), comparable ratios have been deduced for the high-slip patches of the 2004 Sumatra and 2011 Tohoku tsunamigenic earthquakes and for the great 1897 Assam earthquake (e.g. [72,77–79]).

In figures 6–9, we illustrate maximum wave heights generated by these sources; we also calculate, for each longitude around the northern shore of Africa and each latitude along the eastern shore of the Mediterranean, the wave height at the location where the water depth shallows to 50 m, showing those calculations as bordering panels in figures 6–9.

Although there is uncertainty in the assumed lengths of, and slips on, the fault segments, this uncertainty is to some extent mitigated by the recognition that our calculations may, with caveats, be re-scaled to take account of different magnitudes of slip and to deal with different lengths of fault segment. In the open ocean, tsunamis propagate in a linear fashion (e.g. [80]), and we should expect the wave height to scale linearly with the slip in the earthquake if the other source parameters remain constant. Re-scaling is also possible for sources of different lengths. We illustrate this point by comparing wave heights at the 50 m isobath calculated for the sources of Shaw *et al.* [10] and Papadimitriou & Karakostas [8] (sources 1 and 2, figure 4 and table 1). These two sources are similar in all their parameters, with the exception that they differ in length by a factor of 1.5, such that the area of sea floor that is lifted up by source 2 is 1.5 times greater than for source 1. Figure 6*b* shows that the wave heights generated by source 2 are approximately 1.5 times the height of the waves generated by source 1. Another example of this scaling is given in Figure S6 of the electronic supplementary material, where two candidate sources for a tsunamigenic earthquake near Rhodes, which differ in strike by about 10° and in seismic moment by a factor of 4.5, yield very similar scaled distributions of wave heights.

More generally, the amount of gravitational potential energy put into the water column by slip in an earthquake is proportional to the fault area and to the magnitude of the vertical component of the slip. The product of these two quantities is the scalar moment of the earthquake multiplied

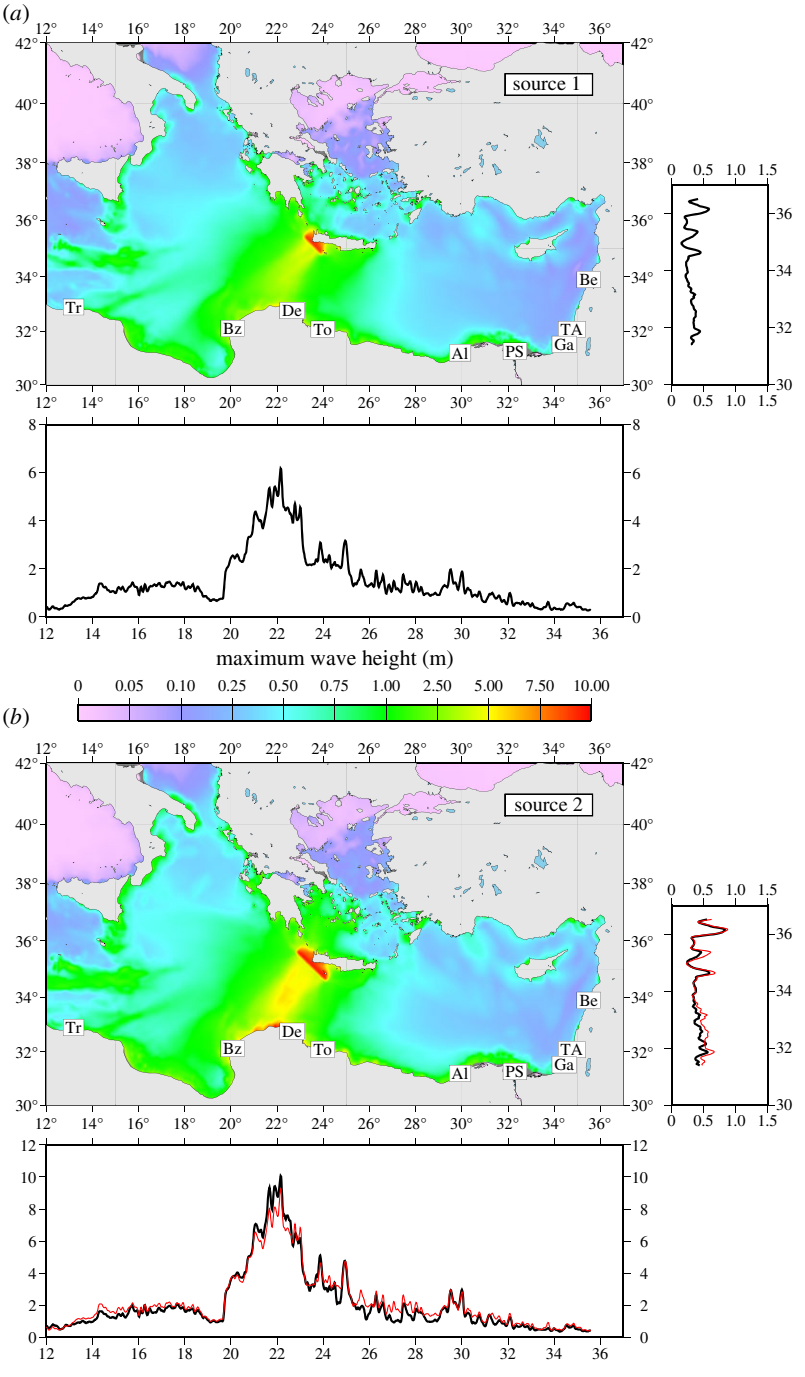

Figure 6. Hydrodynamic calculations of maximum wave heights (above undisturbed sea level) in the Eastern Mediterranean basin and profiles of maximum wave height along near-shore 50 m isobaths, for sources near western Crete. Colours (colour scale in centre) display the maximum height of the sea surface above its undisturbed level in the 4 h following the uplift of the sea floor that initiates the calculation. Bordering panels show maximum wave height in metres, for that same interval, recorded along the 50 m isobath near the coast of Africa (bottom panel) and the Levant (right-hand panel). In (*b*) black lines are calculated for source 2 (table 1) with 20 m of slip; the red lines represent wave heights calculated from source 1, also with 20 m of slip, but with their amplitudes multiplied by a factor of 1.5 (which represents the ratio of the seismic moment of the two sources). The locations of cities referred to in figure 10 are denoted by two-letter abbreviations: Tr, Tripoli; Bz, Benghazi; De, Derna; To, Tobruk; Al, Alexandria; PS, Port Said; Ga, Gaza; TA, Tel Aviv; Be, Beirut.

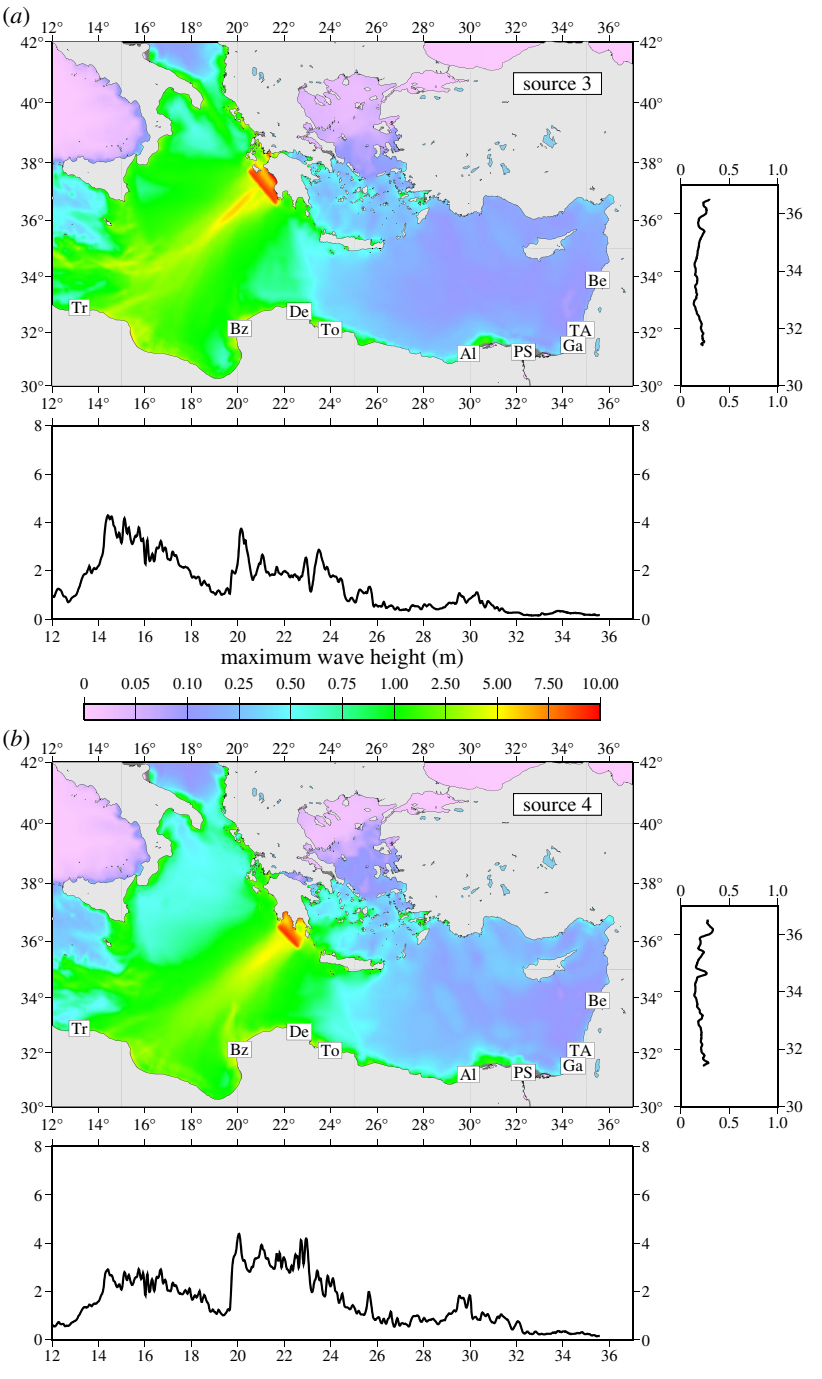

Figure 7. As figure 6 for sources near the Peloponnese (figure 5*a*).

by the sine of the dip of the fault and divided by the shear modulus [81]. For earthquake sources in approximately the same region, i.e. with approximately the same distributions of water depth, then the amount of energy put into the water column by an earthquake depends only upon its scalar moment and the dip. We should expect small-scale differences between sources to disperse during propagation, and then, provided that the sources we consider are all long in comparison with the water depth, for fixed fault orientation, we should expect wave heights to scale with the moment, as just described.

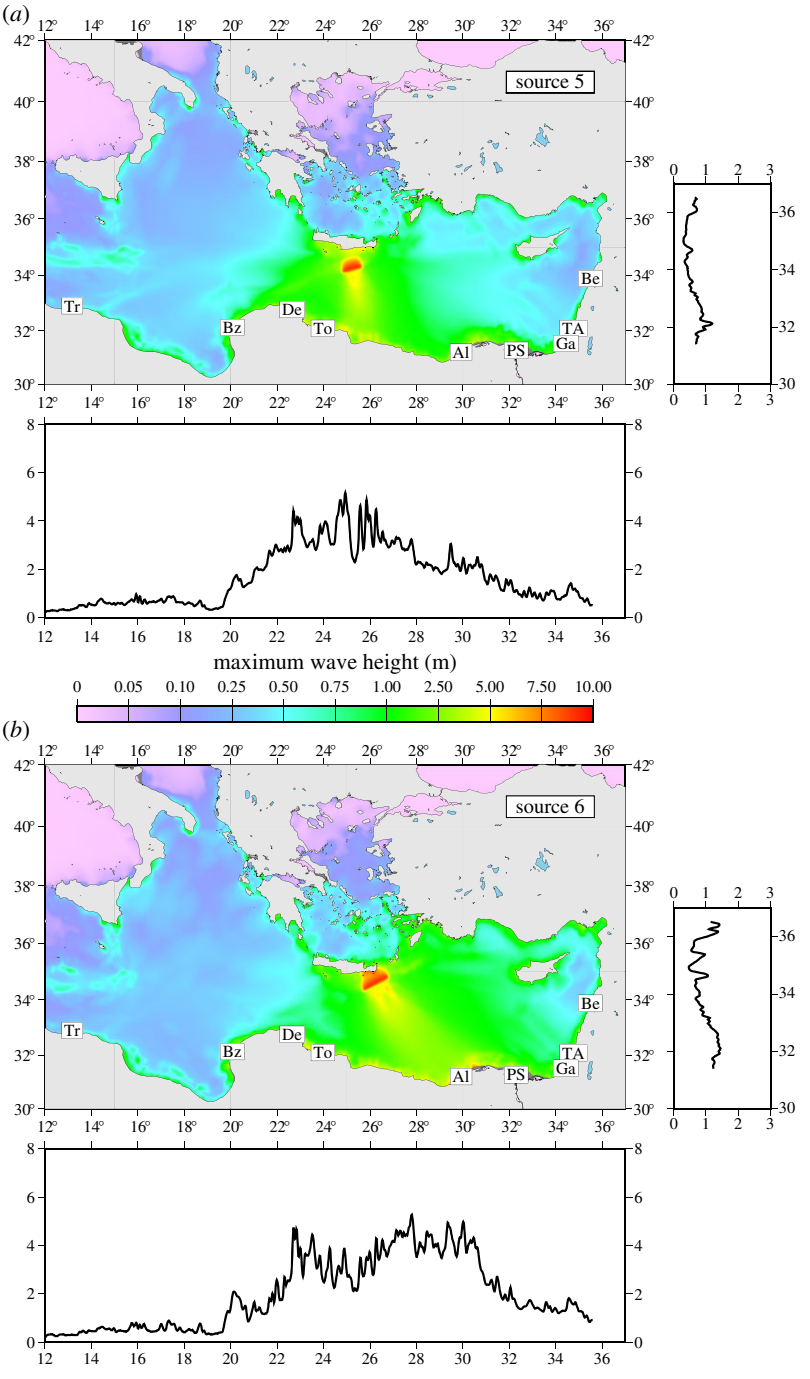

Figure 8. As figure 7 for sources near eastern Crete (figure 4).

Clearly, such scaling applies only to sources having the same strike and lying in close proximity to one another. We also emphasize that, because propagation becomes pronouncedly nonlinear in shallow water and for inundation of land, our remarks about scaling do not apply to water shallower than the 50 m isobath illustrated in figures 6–9. Accurate analysis of run-up and inundation requires detailed knowledge of local bathymetry and land conditions, which are not available to us.

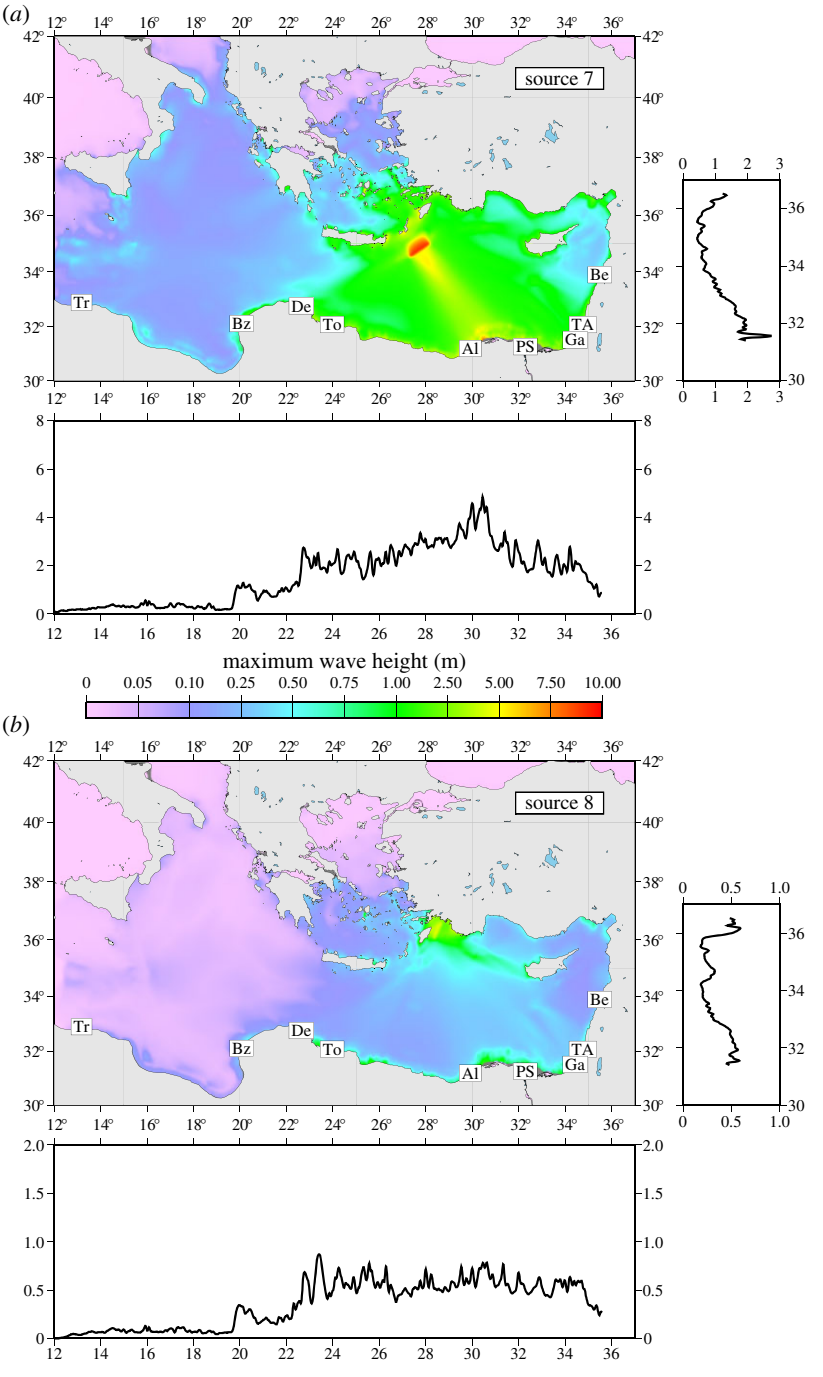

Figure 9. As figure 7 for sources at the eastern end of the Hellenic plate boundary (figure 5*b*).

A significant difference between our study and earlier studies of the propagation of tsunamis from the Hellenic plate boundary arises from our recognition of variation by almost 90° in the strike of potential sources along the boundary. The waves of greatest height propagate along the relatively short paths between sources and the opposite side of the Mediterranean, in the direction approximately perpendicular to the strike of the source, with little lateral spreading. In consequence, the distribution of wave heights along the coast of North Africa differs greatly

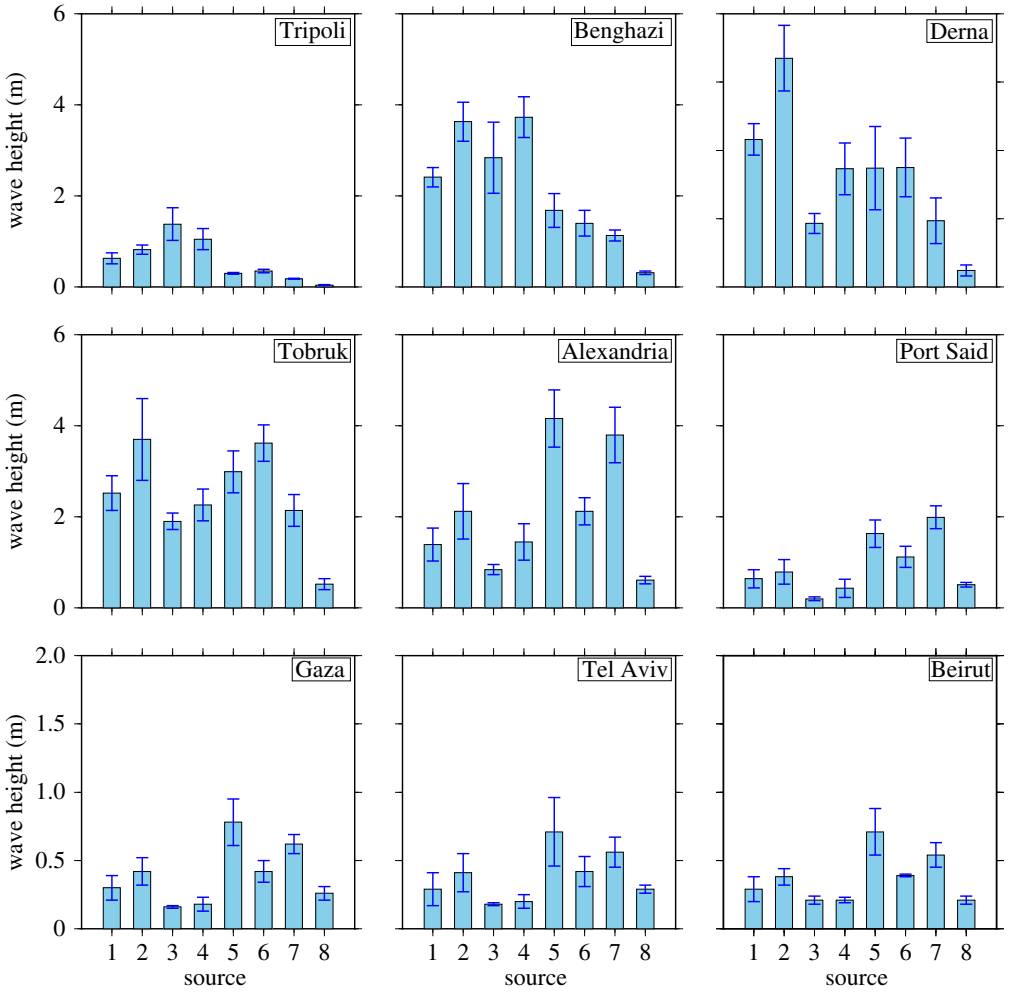

Figure 10. Maximum calculated wave heights at the 50 m isobath near large cities on the coasts of North Africa and the Levant for the eight tsunami sources illustrated in figures 6–9. Bars show the average of the maximum wave height for the points on the 50 m isobath within 25 km of the city; error symbols show the range of ± 2 s.d. in those measurements. Note that the vertical scales differ. These calculations cannot be used to make estimates of run-up and inundation; however, calculated wave heights of over 1 m indicate the possibility of substantial flooding. (Online version in colour.)

between sources in western Crete (figure 6) and those nearby in the Peloponnese (figure 7). Even the relatively small difference in strike between the two model source segments beneath eastern Crete (figure 4) results in appreciably different distributions of wave height along the coast of Egypt (figure 8).

Figure 10 shows the maximum wave heights at the 50 m isobath for nine large cities along the coast of North Africa and the Levant, calculated for the eight sources listed in table 1. All these calculations are for a standard slip (table 1). As discussed above, it is not possible to convert these wave heights into accurate estimates of run-up without further detailed calculations employing high-resolution, high-precision maps of near-shore bathymetry. We may, nevertheless, make comparisons among the different sites. Recall that Alexandria and much of the Nile Delta were devastated by the AD 365 tsunami [6,50,51], which was generated by an earthquake similar to sources 1 and 2. The wave heights offshore from Alexandria calculated from those sources are about 2 m (figure 10). Wave heights off Benghazi, Derna and Tobruk exceed 2 m for all of the

sources except source 8, and the calculated wave heights off Alexandria for sources 5, 6 and 7, near eastern Crete and Karpathos (figures 4 and 5), are also higher than those calculated for the source of AD 365.

The wave heights calculated for Port Said and the Levantine coast are generally lower than 1 m, and any assessment of tsunami hazard in this region must also take account of tsunami sources local to that region [49], which are beyond the scope of this paper.

5. Discussion and conclusion

Studies of tsunami hazard commonly start with a model that is strongly constrained by the locations of earthquakes that have occurred in the 50 years or so during which worldwide seismic networks have been operating, though such models may be modified by information drawn from fault maps (e.g. [1–3,82]). The observations that we summarize here suggest that it would be unwise to treat seismological data as the primary source of information for estimating tsunami hazard in the Eastern Mediterranean. Most of the deformation across the Hellenic plate boundary is aseismic [17], and we are aware of no clear evidence from seismology alone for the existence of the faults that slipped in the tsunamigenic earthquakes of AD 365 or AD 1303.

Here, we have taken an approach that is based on combining geological, geodetic, geomorphological, geochronological, historical and seismological data to form a model of the tsunamigenic potential of the plate boundary (e.g. [6,7,10–14,19–21,25,29,31]). The central aspects of this model are that the subduction fault itself slips in a predominantly aseismic fashion, and that the tsunami hazard is associated with more steeply dipping faults within the accretionary prism on top of the Nubian plate, which deliver rare great earthquakes [8,10–12,53]. One of these faults crops out along the prominent bathymetric scarp of the 400 km-long Hellenic Trench. Analysis of uplift in the AD 365 earthquake suggests that, at least beneath western Crete, this fault dips approximately at 30° to a depth of 40–45 km [8,10]. Although this fault bears some resemblance to 'splays' that have been associated with actual or potential tsunamis in other subduction zones (e.g. [83–86]), it differs from them in that it seems to be the primary seismic and tsunamigenic fault, from the surface to a depth of 40–45 km. The faulting at the eastern end of the Hellenic plate boundary is more uncertain, and perhaps more complicated. Here, the overall relative motion is highly oblique, but the slip vectors of earthquakes near the top of the Nubian plate indicate that slip may be partitioned, with the transcurrent component of motion taking place on the subduction fault while the contractional component is absorbed on one or more faults within the upper plate ([13] and figures 3, 4 and 5*b*).

We have carried out simulations of tsunamis generated by candidate earthquake sources around the Hellenic plate boundary (table 1). In two cases, the sources are constrained by detailed studies: of the AD 365 earthquake in western Crete [8,10,12], and of the earthquake in Roman or Bronze Age time near Rhodes [13–16]. In the remaining cases, the locations are decided primarily on the basis of geomorphological expressions of faulting. Although there are uncertainties attached to this procedure, the orientations of individual fault segments are well constrained by prominent bathymetric scarps with which they are associated (figures 4 and 5). For a given orientation of fault segment, the calculated wave heights scale, to a good approximation, with the moment of the causative earthquake (see discussion of figure 6).

Much attention has been paid recently to the uncertainties involved in calculating run-up and inundation for a given tsunami source. In the Eastern Mediterranean at least, the dominant uncertainties are those associated with the source itself. For any given location on the coast of North Africa, the impact of a tsunami is dependent principally upon the moment of the causative earthquake, and upon where along the Hellenic plate boundary the earthquake occurs (which determines the orientation of the fault, hence the direction in which the greatest energy propagates in the tsunami, compare figures 6–9). We remind the reader that the near-shore wave heights calculated in those figures cannot be translated directly into predictions of run-up, for the reasons discussed in §4. A sensible approach is to recognize that the AD 365 and AD 1303 earthquakes caused devastating tsunamis on the coast of Africa and that similarly

sized earthquakes in the future will probably do the same. Our calculations should be taken as showing, for a given location of tsunamigenic earthquake, which locations are likely to suffer more than others.

Finally, we contend that a probabilistic assessment of tsunami hazard in the Eastern Mediterranean would, given the present state of knowledge, be misguided. As we mention above, measurements of seismicity in the Hellenic plate boundary over the past few decades are largely, perhaps totally, irrelevant to the faults that cause the tsunamis. Although some certainty attaches to the locations of the hazardous faults, the estimates from GPS of the contractional strain that will eventually be released in earthquakes along those faults differ by a factor of 10 or more [10,21,87]. Given such uncertainties, it is prudent to take a precautionary approach to the hazard.

Authors' contributions. This project arose from discussions, over several years, between P.E., J.J. and C.S. The calculations were carried out by A.H. in collaboration with C.S. The first draft of the manuscript was written by P.E., and the other authors commented on and contributed to the final paper.

Competing interests. We declare we have no competing interests.

Funding. This work was supported by the Natural Environmental Research Council through grant no. NE/J02001X/1. C.S.'s work was funded by the FP7 programme ASTARTE. A.H. is supported by a Shell Scholarship.

Acknowledgements. We benefited from many discussions with B. Shaw, T. Higham, N. Kalligeris and the late N. N. Ambraseys. We are grateful to R. Bilham for a helpful review, and for suggesting figure 10; we also thank an anonymous reviewer for their detailed and thoughtful review. Most of the figures were made using the Generic Mapping Tools [88].

References

1. Lorito S, Tiberti MM, Basili R, Piatanesi A, Valensise G. 2008 Earthquake-generated tsunamis in the Mediterranean Sea: scenarios of potential threats to southern Italy. *J. Geophys. Res.* **113**, B01301. (doi:10.1029/2007JB004943)
2. Tinti S, Armigliato A, Pagnoni G, Zaniboni F. 2005 Scenarios of giant tsunamis of tectonic origin in the Mediterranean. *ISET J. Earthq. Technol.* **42**, 171–188. See http://home.iitk.ac.in/~vinaykg/Iset464.pdf.
3. Sørensen MB, Spada M, Babeyko A, Wiemer S, Grünthal G. 2012 Probabilistic tsunami hazard in the Mediterranean Sea. *J. Geophys. Res.* **117**, B01305. (doi:10.1029/2010JB008169)
4. Valle BL, Kalligeris N, Findikakis AN, Okal EA, Melilla L, Synolakis CE. 2014 Plausible megathrust tsunamis in the eastern Mediterranean Sea. *Proc. Inst. Civil Eng. – Eng. Comput. Mech.* **167**, 99–105. (doi:10.1680/eacm.13.00027)
5. Yolsal S, Taymaz T, Yalçiner X. 2007 Understanding tsunamis, potential source regions and tsunami-prone mechanisms in the Eastern Mediterranean. *Geol. Soc. Lond. Spec. Publ.* **291**, 201–230. (doi:10.1144/SP291.10)
6. Ambraseys NN. 2009 *Earthquakes in the Mediterranean and Middle East*. Cambridge, UK: Cambridge University Press.
7. Ambraseys N, Synolakis C. 2010 Tsunami catalogs for the Eastern Mediterranean, revisited. *J. Earthq. Eng.* **14**, 309–330. (doi:10.1080/13632460903277593)
8. Papadimitriou EE, Karakostas VG. 2008 Rupture model of the great AD 365 Crete earthquake in the southwestern part of the Hellenic Arc. *Acta Geophys.* **56**, 293–312. (doi:10.2478/s11600-008-0001-6)
9. Pirazzoli PA, Laborel J, Stiros S. 1996 Earthquake clustering in the eastern Mediterranean during historical times. *J. Geophys. Res.* **101**, 6083–6098. (doi:10.1029/95JB00914)
10. Shaw B *et al.* 2008 Eastern Mediterranean tectonics and tsunami hazard inferred from the AD 365 earthquake. *Nat. Geosci.* **1**, 268–276. (doi:10.1038/ngeo151)
11. Stiros S. 2001 The AD 365 Crete earthquake and possible seismic clustering during the fourth to sixth centuries AD in the eastern Mediterranean: a review of historical and archaeological data. *J. Struct. Geol.* **23**, 545–562. (doi:10.1016/S0191-8141(00)00118-8)
12. Stiros SC, Drakos A. 2006 A fault model for the tsunami-associated, magnitude ≥ 8.5 Eastern Mediterranean, AD 365 earthquake. In *Tsunamis, hurricanes and neotectonics as driving mechanisms in coastal evolution* (eds A Scheffers, D Kelletat), Z. Geomorphol. Suppl. Vol. 146, pp. 125–137. Berlin, Germany: Borntraeger.

13. Howell A, Jackson J, England P, Higham T, Synolakis C. In press. Late Holocene uplift of Rhodes, Greece: evidence for a large tsunamigenic earthquake and the implications for the tectonics of the eastern Hellenic Trench system. *Geophys. J. Int*. See http://www.repository.cam.ac.uk/handle/1810/249094.
14. Kontogianni V, Tsoulos N, Stiros S. 2002 Coastal uplift, earthquakes and active faulting of Rhodes Island (Aegean Arc): modeling based on geodetic inversion. *Mar. Geol.* **186**, 299–317. (doi:10.1016/S0025-3227(02)00334-1)
15. Pirazzoli PA, Montaggioni LF, Saliège JF, Segonzac G, Thommeret Y, Vergnaud-Grazzini C. 1989 Crustal block movements from Holocene shorelines: Rhodes island (Greece). *Tectonophysics* **170**, 89–114. (doi:10.1016/0040-1951(89)90105-4)
16. Stiros S, Blackman DJ. 2013 Seismic coastal uplift and subsidence in Rhodes Island, Aegean arc: evidence from an uplifted ancient harbour. *Tectonophysics* **611**, 114–120. (doi:10.1016/j.tecto.2013.11.020)
17. Jackson J, McKenzie DP. 1988 The relationship between plate motions and seismic moment tensors, and the rates of active deformation in the Mediterranean and Middle East. *Geophys. J. Int.* **93**, 45–73. (doi:10.1111/j.1365-246X.1988.tb01387.x)
18. Benetatos C, Kiratzi A, Papazachos C, Karakaisis G. 2004 Focal mechanisms of shallow and intermediate depth earthquakes along the Hellenic Arc. *J. Geodyn.* **37**, 253–296. (doi:10.1016/j.jog.2004.02.002)
19. Caputo R, Catalano S, Monaco C, Romagnoli G, Tortorici G, Tortorici L 2010 Active faulting on the island of Crete (Greece). *Geophys. J. Int.* **183**, 111–126. (doi:10.1111/j.1365-246X.2010.04749.x)
20. Shaw B, Jackson J. 2010 Earthquake mechanisms and active tectonics of the Hellenic subduction zone. *Geophys. J. Int.* **181**, 966–984. (doi:10.1111/j.1365-246X.2010.04551.x)
21. Vernant P, Reilinger R, McClusky S. 2014 Geodetic evidence for low coupling on the Hellenic subduction plate interface. *Earth Planet. Sci. Lett.* **385**, 122–129. (doi:10.1016/j.epsl.2013.10.018)
22. Nocquet J-M. 2012 Present-day kinematics of the Mediterranean: a comprehensive overview of GPS results. *Tectonophysics* **579**, 220–242. (doi:10.1016/j.tecto.2012.03.037)
23. Reilinger R *et al.* 2006 GPS constraints on continental deformation in the Africa–Arabia–Eurasia continental collision zone and implications for the dynamics of plate interactions. *J. Geophys. Res.* **111**, B05411. (doi:10.1029/2005JB004051)
24. Aktuğ B *et al.* 2009 Deformation of western Turkey from a combination of permanent and campaign GPS data: limits to block-like behavior. *J. Geophys. Res.* **114**, B10404. (doi:10.1029/2008JB006000)
25. Floyd MA *et al.* 2010 A new velocity field for Greece: implications for the kinematics and dynamics of the Aegean. *J. Geophys. Res.* **115**, B10403. (doi:10.1029/2009JB007040)
26. Engdahl E, van der Hilst R, Buland R. 1998 Global teleseismic earthquake relocation with improved travel times and procedures for depth determination. *Bull. Seismol. Soc. Amer.* **88**, 722–743. See http://www.bssaonline.org/content/88/3/722/.
27. International Seismological Centre. 2011 *EHB Bulletin*. International Seismological Centre, Thatcham, UK. See http://www.isc.ac.uk.
28. Engdahl ER, Villaseñor A. 2002 Global seismicity: 1900–1999. In *IASPEI handbook of earthquake and engineering seismology, part A* (eds WHK Lee, P Jennings, H Kanamori, C Kisslinger), pp. 665–690. Boston, MA: Academic Press.
29. Ambraseys N, Jackson JA. 1998 Faulting associated with historical and recent earthquakes in the Eastern Mediterranean region. *Geophys. J. Int.* **133**, 390–406. (doi:10.1046/j.1365-246X.1998.00508.x)
30. Taymaz T, Jackson J, McKenzie D. 1991 Active tectonics of the north and central Aegean Sea. *Geophys. J. Int.* **106**, 433–490. (doi:10.1111/j.1365-246X.1991.tb03906.x)
31. Jackson J. 1994 Active tectonics of the Aegean region. *Annu. Rev. Earth Planet. Sci.* **22**, 239–271. (doi:10.1146/annurev.ea.22.050194.001323)
32. Armijo R, Lyon-Caen H, Papanastassiou D. 1992 East–west extension and Holocene normal-fault scarps in the Hellenic arc. *Geology* **20**, 491–494. (doi:10.1130/0091-7613(1992)020<0491:EWEAHN>2.3.CO;2)
33. Huchon P, Lybéris N, Angelier J, Pichon XL, Renard V. 1982 Tectonics of the Hellenic Trench: a synthesis of Sea-Beam and submersible observations. *Tectonophysics* **86**, 69–112. (doi:10.1016/0040-1951(82)90062-2)

34. Kiratzi A. 2013 The January 2012 earthquake sequence in the Cretan Basin, south of the Hellenic volcanic arc: focal mechanisms, rupture directivity and slip models. *Tectonophysics* **586**, 160–172. (doi:10.1016/j.tecto.2012.11.019)
35. Chaumillon E, Mascle J. 1997 From foreland to forearc domains: new multichannel seismic reflection survey of the Mediterranean ridge accretionary complex (Eastern Mediterranean). *Mar. Geol.* **138**, 237–259. (doi:10.1016/S0025-3227(97)00002-9)
36. Huguen C, Mascle J, Chaumillon E, Woodside JM, Benkhelil J, Kopf A, Volkonskaïa A 2001 Deformational styles of the eastern Mediterranean Ridge and surroundings from combined swath mapping and seismic reflection profiling. *Tectonophysics* **343**, 21–47. (doi:10.1016/S0040-1951(01)00185-8)
37. Mascle J, Chaumillon E. 1998 An overview of Mediterranean Ridge collisional accretionary complex as deduced from multichannel seismic data. *Geo-Mar. Lett.* **18**, 81–89. (doi:10.1007/s003670050056)
38. Le Pichon X, Angelier J. 1979 The Hellenic Trench system: a key to the neotectonic evolution of the Eastern Mediterranean area. *Tectonophysics* **60**, 1–42. (doi:10.1016/0040-1951(79)90131-8)
39. Kreemer C, Chamot-Rooke N. 2004 Contemporary kinematics of the southern Aegean and the Mediterranean Ridge. *Geophys. J. Int.* **157**, 1377–1392. (doi:10.1111/j.1365-246X.2004.02270.x)
40. Mascle J, Cleac'h A, Jongsma D. 1986 The eastern Hellenic margin from Crete to Rhodes: example of progressive collision. *Mar. Geol.* **73**, 145–168. (doi:10.1016/0025-3227(86)90116-7)
41. McKenzie D. 1978 Active tectonics of the Alpine–Himalayan belt: the Aegean sea and surrounding regions. *Geophys. J. Int.* **55**, 217–254. (doi:10.1111/j.1365-246X.1978.tb04759.x)
42. Gallen SF, Wegmann KW, Bohnenstiehl DR, Pazzaglia FJ, Brandon MT, Fassoulas C 2014 Active simultaneous uplift and margin-normal extension in a forearc high, Crete, Greece. *Earth Planet. Sci. Lett.* **398**, 11–24. (doi:10.1016/j.epsl.2014.04.038)
43. Mascle J, Jongsma D, Campredon R, Dercourt J, Glaçon G, Lecleach A, Lybéris N, Malod JA, Mitropoulos D 1982 The Hellenic margin from eastern Crete to Rhodes: preliminary results. *Tectonophysics* **86**, 133–147. (doi:10.1016/0040-1951(82)90064-6)
44. Özbakır AD, Şengör AMC, Wortel MJR, Govers R. 2013 The Pliny–Strabo trench region – a large shear zone resulting from slab tearing. *Earth Planet. Sci. Lett.* **375**, 188–195. (doi:10.1016/j.epsl.2013.05.025)
45. Jongsma D. 1977 Bathymetry and shallow structure of the Pliny and Strabo Trenches, south of the Hellenic Arc. *Geol. Soc. Amer. Bull.* **88**, 797–805. (doi:10.1130/0016-7606(1977)88<797:BASSOT>2.0.CO;2)
46. Peters J, Huson W. 1985 The Pliny and Strabo trenches (eastern Mediterranean): integration of seismic reflection data and SeaBeam bathymetric maps. *Mar. Geol.* **64**, 1–17. (doi:10.1016/0025-3227(85)90157-4)
47. tenVeen JH, Boulton SJ, Alçiçek MC. 2009 From palaeotectonics to neotectonics in the Neotethys realm: the importance of kinematic decoupling and inherited structural grain in SW Anatolia (Turkey). *Tectonophysics* **473**, 261–281. (doi:10.1016/j.tecto.2008.09.030)
48. Taymaz T, Jackson J, Westaway R. 1990 Earthquake mechanisms in the Hellenic Trench near Crete. *Geophys. J. Int.* **102**, 695–731. (doi:10.1111/j.1365-246X.1990.tb04590.x)
49. Salamon A, Rockwell T, Ward SN, Guidoboni E, Comastri A. 2007 Tsunami hazard evaluation of the eastern Mediterranean: historical analysis and selected modeling. *Bull. Seismol. Soc. Amer.* **97**, 705–724. (doi:10.1785/0120060147)
50. Ambraseys N, Melville C, Adams RD. 1994 *The seismicity of Egypt, Arabia and the Red Sea: a historical review*. Cambridge, UK: Cambridge University Press.
51. Guidoboni E, Comastri A, Traina G. 1994 *Catalogue of ancient earthquakes in the Mediterranean Area up to the 10th century*. Bologna, Italy: Istituto Nazionale di Geofisica.
52. Pirazzoli P. 1986 The Early Byzantine tectonic paroxysm. In *Dating Mediterranean shorelines* (eds A Ozer, C Vita-Finzi), Z. Geomorphol. Suppl. Vol. 62, pp. 31–39. Berlin, Germany: Borntraeger.
53. Pirazzoli PA, Thommeret J, Thommeret Y, Laborel J, Montaggioni LF. 1982 Crustal block movements from Holocene shorelines: Crete and Antikythira. *Tectonophysics* **86**, 27–43. (doi:10.1016/0040-1951(82)90060-9)
54. Spratt TAB. 1865 *Travels and researches in Crete*, vol. 2. London, UK: J. van Voorst.
55. Pirazzoli PA, Laborel J, Stiros SC. 1996 Coastal indicators of rapid uplift and subsidence: examples from Crete and other Eastern Mediterranean sites. In *Field methods and models to*

quantify rapid coastal changes (eds D Kelletat, NP Psuty), Z. Geomorphol. Suppl. Vol. 102, pp. 21–35. Berlin, Germany: Borntraeger.
56. Driessen J, Macdonald CF. 1997 *The troubled island: Minoan Crete before and after the Santorini eruption*. Aegaeum, vol. 17. Liège, Belgium: Université de Liège.
57. Shaw B, Jackson JA, Higham TFG, England PC, Thomas AL. 2010 Radiometric dates of uplifted marine fauna in Greece: implications for the interpretation of recent earthquake and tectonic histories using lithophagid dates. *Earth Planet. Sci. Lett.* **297**, 395–404. (doi:10.1016/j.epsl.2010.06.041)
58. Gaki-Papanastassiou K, Karymbalis E, Papanastassiou D, Maroukian H. 2009 Quaternary marine terraces as indicators of neotectonic activity of the Ierapetra normal fault SE Crete (Greece). *Geomorphology* **104**, 38–46. (doi:10.1016/j.geomorph.2008.05.037)
59. Peters JM, Troelstra SR, van Harten D. 1985 Late Neogene and Quaternary vertical movements in eastern Crete and their regional significance. *J. Geol. Soc. Lond.* **142**, 501–513. (doi:10.1144/gsjgs.142.3.0501)
60. Guidoboni E, Comastri A. 1997 The large earthquake of 8 August 1303 in Crete: seismic scenario and tsunami in the Mediterranean area. *J. Seismol.* **1**, 55–72. (doi:10.1023/A:1009737632542)
61. Monaco C, Tortorici L. 2004 Faulting and effects of earthquakes on Minoan archaeological sites in Crete (Greece). *Tectonophysics* **382**, 103–116. (doi:10.1016/j.tecto.2003.12.006)
62. Manning S, Ramsey CB, Kutschera W, Higham T, Kromer B, Steier P, Wild EM. 2006 Chronology for the Aegean Late Bronze Age 1700–1400 BC. *Science* **312**, 565–569. (doi:10.1126/science.1125682)
63. Dalmayrac B, Molnar P. 1981 Parallel thrust and normal faulting in Peru and constraints on the state of stress. *Earth Planet. Sci. Lett.* **55**, 473–481. (doi:10.1016/0012-821X(81)90174-6)
64. Farías M, Comte D, Roecker S, Carrizo D, Pardo M. 2011 Crustal extensional faulting triggered by the 2010 Chilean earthquake: the Pichilemu seismic sequence. *Tectonics* **30**, TC6010. (doi:10.1029/2011TC002888)
65. Stiros SC, Pirazzoli PA, Fontugne M. 2009 New evidence of Holocene coastal uplift in the Strophades Islets (W Hellenic Arc, Greece). *Mar. Geol.* **267**, 207–211. (doi:10.1016/j.margeo.2009.09.002)
66. Kelletat D, Kowalczyk G, Schröder B, Winter K. 1976 A synoptic view of the neotectonic development of the Peloponnesian coastal regions. *Z. Deutsche Geol. Ges.* **27**, 447–465.
67. Okada Y. 1992 Internal deformation due to shear and tensile faults in a half-space. *Bull. Seismol. Soc. Amer.* **82**, 1018–1040. See http://www.bssaonline.org/content/82/2/1018.abstract/.
68. Flouri ET, Kalligeris N, Alexandrakis G, Kampanis NA, Synolakis CE. 2013 Application of a finite difference computational model to the simulation of earthquake generated tsunamis. *Appl. Numer. Math.* **67**, 111–125. (doi:10.1016/j.apnum.2011.06.003)
69. Synolakis CE, Bernard EN, Titov VV, Kânoğlu U, González FI. 2008 Validation and verification of tsunami numerical models. *Pure Appl. Geophys.* **165**, 2197–2228. (doi:10.1007/s00024-004-0427-y)
70. Titov V, Synolakis C. 1998 Numerical modeling of tidal wave runup. *J. Waterway Port Coastal Ocean Eng.* **124**, 157–171. (doi:10.1061/(ASCE)0733-950X(1998)124:4(157))
71. Oldham RD. 1899 Report on the great earthquake of 12th June 1897. *Mem. Geol. Surv. India* **29**, 1–379.
72. Bilham R, England P. 2001 Plateau 'pop-up' in the great 1897 Assam earthquake. *Nature* **410**, 806–809. (doi:10.1038/35071057)
73. Chabalier JB, Lyon-Caen H, Zollo A, Deschamps A, Bernard P, Hatzfeld D 1992 A detailed analysis of microearthquakes in western Crete from digital three-component seismograms. *Geophys. J. Int.* **110**, 347–360. (doi:10.1111/j.1365-246X.1992.tb00879.x)
74. Meier T, Rische M, Endrun B, Vafdis A, Harjes H-P. 2004 Seismicity of the Hellenic subduction zone in the area of western and central Crete observed by temporary local seismic networks. *Tectonophysics* **383**, 149–169. (doi:10.1016/j.tecto.2004.02.004)
75. Tichelaar BW, Ruff L. 1993 Depth of seismic coupling along subduction zones. *J. Geophys. Res.* **98**, 2107–2037. (doi:10.1029/92JB02045)
76. Wells D, Coppersmith K. 1994 New empirical relationships among magnitude, rupture length, rupture width, rupture area, and surface displacement. *Bull. Seismol. Soc. Amer.* **84**, 974–1002. See http://www.bssaonline.org/content/84/4/974.abstract/.

77. Koketsu K *et al.* 2011 A unified source model for the 2011 Tohoku earthquake. *Earth Planet. Sci. Lett.* **310**, 480–487. (doi:10.1016/j.epsl.2011.09.009)
78. Subarya C, Chlieh M, Prawirodirdjo L, Avouac J-P, Bock Y, Sieh K, Meltzner AJ, Natawidjaja DH, McCaffrey R 2006 Plate-boundary deformation associated with the great Sumatra–Andaman earthquake. *Nature* **440**, 46–51. (doi:10.1038/nature04522)
79. Yue H, Lay T. 2013 Source rupture models for the M_w 9.0 2011 Tohoku earthquake from joint inversions of high-rate geodetic and seismic data. *Bull. Seismol. Soc. Am.* **103**, 1242–1255. (doi:10.1785/0120120119)
80. Synolakis C, Bernard E. 2006 Tsunami science before and beyond Boxing Day 2004. *Phil. Trans. R. Soc. A* **364**, 2231–2265. (doi:10.1098/rsta.2006.1824)
81. Aki K, Richards PG. 2002 *Quantitative seismology*, 2nd edn. Sausalito, CA: University Science Books.
82. Basili R, Tiberti MM, Kastelic V, Romano F, Piatanesi A, Selva J, Lorito S. 2013 Integrating geologic fault data into tsunami hazard studies. *Nat. Hazards Earth Syst. Sci.* **13**, 1025–1050. (doi:10.5194/nhess-13-1025-2013)
83. Chapman JB, Elliott J, Doser DI, Pavlis TL. 2014 Slip on the Suckling Hills splay fault during the 1964 Alaska earthquake. *Tectonophysics* **637**, 191–197. (doi:10.1016/j.tecto.2014.10.007)
84. Moore GF, Bangs NL, Taira A, Kuramoto S, Pangborn E, Tobin HJ. 2007 Three-dimensional splay fault geometry and implications for tsunami generation. *Science* **318**, 1128–1131. (doi:10.1126/science.1147195)
85. Park J, Tsuru T, Kodaira S, Cummins P, Kaneda Y. 2002 Splay fault branching along the Nankai subduction zone. *Science* **297**, 1157–1160. (doi:10.1126/science.1074111)
86. Strasser M *et al.* 2009 Origin and evolution of a splay fault in the Nankai accretionary wedge. *Nat. Geosci.* **2**, 648–652. (doi:10.1038/ngeo609)
87. Ganas A, Parsons T. 2009 Three-dimensional model of Hellenic Arc deformation and origin of the Cretan uplift. *J. Geophys. Res.* **114**, B06404. (doi:10.1029/2008JB005599)
88. Wessel P, Smith WHF, Scharroo R, Luis J, Wobbe F. 2013 Generic Mapping Tools: improved version released. *EOS Trans. Amer. Geophys. Union* **94**, 409–410. (doi:10.1002/2013EO450001)